STM JOURNALS

Journal of
Polymer & Composites

ISSN: 2321-2810 (Online)
ISSN: 2321-8525 (Print)
Volume 12, Special Issue 5, 2024
DOI (Journal): 10.37591/JoPC

http://engineeringjournals.stmjournals.in/index.php/JoPC/index

Research JoPC

Numerical Investigation on Structural Behavior of RC Beam-Column Joints: Beam Weak in Shear

Mayank Kumar Thakur[1,*], P. Poluraju[2]

Abstract

This study presents a numerical investigation on structural performance of reinforced concrete (RC) beam-column joints (BCJ) with beam weak in shear subjected to cyclic loading. Retrofitting techniques are explored, utilizing Glass Fiber Reinforced Polymer (GFRP) for shear strengthening, in accordance with ductile detailing standards outlined in IS 13920:2016. The column and beam elements are designed following the guidelines of IS 456:2000. Various specimen scales, including full-scale, $^{2}/_{3}$-scale, and $^{1}/_{3}$-scale specimens, are employed for comprehensive analysis. Two main scenarios are considered: firstly, employing 100% shear reinforcement in the beam; and secondly, a mixed approach with 70% shear reinforcement in the beam and 50% shear reinforcement in the column. The study aims to assess the effectiveness of GFRP retrofitting in enhancing the shear capacity of beams while evaluating the influence of different reinforcement configurations on the overall structural performance of RC beam-column joints subjected to cyclic loading. Research on joint behavior in BCJs has dived into the significant dynamics of BCJs, enhancing our grasp of their failure mechanisms and performance across various load conditions. Moreover, investigations into shear strength have contributed to refining design principles and retrofitting methods aimed at improving the resilience and ductility of BCJs. It is concluded that the GFRP wrapping has enhanced the shear strength of beam as well as joint.

Keywords: Beam-column joints, GFRP, numerical investigation, shear strength, retrofitting techniques

INTRODUCTION

Recent earthquake damage is mainly because of weak columns, strong beams, and not enough support in the joints. Joint shear failures can compromise the ductility of reinforced concrete (RC) moment-resisting frames [1]. Data from recent seismic events suggests that the complete collapse of numerous structures could be linked to a brittle shear failure in the joints exemplified by notable events such as the 2011 Tohoku-Oki earthquake and tsunami, the 2010 Chile earthquake, the 2016 Mexico earthquake, and the latest earthquake in Turkey in 2023 [2]. External beam-column joints are more vulnerable than internal ones because they do not have the four-side partial confinement that beams do, which affects core confinement. Different shear reactions emerge from joint confinement by beams during seismic activity; however, the bond-slip failure mode is similar for both exterior and interior joints. Outdated code provisions lead to inadequate transverse shear reinforcement in reinforced concrete moment-resisting frames. These flaws could seriously impair overall structural ductility by causing shear or bond-slip failures [3].

In earthquake loading simulations for reinforced-concrete structures, it is typical to consider elastic

***Author for Correspondence**
Mayank Kumar Thakur

[1]PG Student, Department of Civil Engineering, Koneru Lakshmaiah Education Foundation (Deemed to be University), Vaddeswaram, Guntur, Andhra Pradesh, India
[2]Professor, Department of Civil Engineering, Koneru Lakshmaiah Education Foundation (Deemed to be University), Vaddeswaram, Guntur, Andhra Pradesh, India

Received Date: May 10, 2024
Accepted Date: July 08, 2024
Published Date: November 25, 2024

Citation: Mayank Kumar Thakur, P. Poluraju. Numerical Investigation on Structural Behavior of RC Beam-Column Joints: Beam Weak in Shear. Journal of Polymer & Composites. 2024; 12(Special Issue 5): S202–S226.

behavior in beam-column joints. However, studies conducted on subassemblies built before the year 1970 indicate that joints with high shear and bond-stress demands and no transverse reinforcement show significant reductions in stiffness and strength. The evolution of modeling approaches for the inelastic response of beam-column joints in reinforced-concrete frames has progressed through various stages, each aiming to capture the complex behavior of these critical structural elements [4].

The behavior of beam-column joints in RC frames under lateral and vertical loads has been a critical point in structural stability. The design philosophy of "strong-column and weak-beam" emphasizes maintaining joint elasticity. In ductile structures, the flexural strength of longitudinal beams exhibits behavior, with a preference for the beam-fail mechanism to preserve deformability without significant resistance capacity loss. Ductile frame design permits plastic hinge development in beams, safeguarding against critical damage to columns and joints. During seismic events, joints face heightened shear forces, demanding substantial bond and shear stresses. The complexities arising from these forces, especially after plastic hinge formation in adjacent beams, underscore the importance of understanding joint shear behavior for assessing overall RC structural performance. Beam-column joints play a pivotal role in the stability of moment-resisting reinforced concrete (RC) frames, especially under combined lateral and vertical loads. Adhering to the design principle of "strong-column and weak-beam," which emphasizes maintaining the joint within the elastic range, is crucial [5].

Stirrups and hoops provide support for horizontal shear reinforcements, while vertical shear is effectively managed by intermediate column bars. As these bars are anticipated to be under compression, they possess ample strength to withstand the tensile stresses generated during the shear-resisting mechanism. The detailing considerations for beam-column joints involve factors such as the arrangement of longitudinal and transverse reinforcement, as well as the required development length for embedded bars. In essence, limitations on the vertical spacing of transverse reinforcement are established in relation to the smallest member dimension, ensuring adequate concrete confinement. Similarly, restrictions are placed based on the diameter of longitudinal column bars to prevent buckling after concrete spalling. The spacing of horizontal lateral reinforcement is more flexible, considering the confinement provided by adjacent members and the distribution of column longitudinal reinforcements. Notably, the spacing of lateral reinforcement remains relatively consistent across all three codes of practice. Stirrups and hoops provide support for horizontal shear, while vertical shear is effectively managed by intermediate column bars. As these bars are anticipated to be under compression, they show sufficient strength to resist the tensile stresses occurred during the shear-resisting mechanism [6].

In a study focused on the experimental verification of RC joints, two distinct types of specimens were prepared. The initial set of joints was carefully crafted with sufficient steel reinforcements, featuring precise detailing at critical sections. In contrast, the second set of samples exhibited deficiencies in beam reinforcement, specifically inadequate bond lengths at the junctions with the columns. When subjected to transverse loading, the first set demonstrated a prolonged plastic zone, indicative of ductile behavior. In contrast, the second set experienced failure attributed to reinforcement pullout, highlighting sudden and non-ductile behavior [7].

Recent seismic events have highlighted the crucial role played by beam-to-column joints in shaping the overall response of RC structures. Over the past two decades, a multitude of theoretical and empirical models have emerged to gauge the shear strength of these joints. A comprehensive overview of the existing models is found in scientific literature that assesses the shear capacity of exterior beam-to-column joints. As the initial phase of a broader analysis, the study assessed and refined these models. Furthermore, the paper quantifies the uncertainties linked to the application of these models, employing established procedures for the probabilistic seismic analysis of structures [8].

The beam-column joint stands as a critical zone in a reinforced concrete frame, experiencing substantial forces during intense ground shaking, thereby significantly impacting the overall structure's response. The conventional assumption of the joint's rigidity overlooks the influence of elevated shear

forces within the joint, leading to brittle shear failure-a structural performance deemed unacceptable, especially in seismic conditions. Consequently, it is crucial to delve into the seismic actions affecting various joint types and emphasize key parameters influencing joint performance, particularly focusing on bond and shear transfer [9].

In a study, it effectively conveys the importance of addressing shear issues in recent seismic incidents. It emphasizes the need for adequate sizing of moment resistance frames and reinforcement of joints during the preliminary design. The consideration of seismic effects in low and medium seismic zones is highlighted, along with the caution that relying on the general code of practice for reinforcement may not meet current seismic codal provisions. The study also appropriately points out the structural inefficiency of beam-column joints when subjected to substantial lateral loads like strong winds, earthquakes, and explosions. The recommendation to include a substantial number of transverse hoops in the joint core for achieving higher strength, stiffness, and ductility during cyclic loading is clear and underscores the importance of specific measures in regions prone to such lateral forces [10].

In a study, the control specimen, lacking shear reinforcement and having inadequate anchorage for the beam's bottom steel bars, underwent a brittle shear failure in the joint, accompanied by slippage of the beam's bottom bars. The bond conditions of the beam's top bars were adversely affected by concrete disintegration in the controlled joint, leading to a significant decrease in both load-carrying capacity and ductility. The use of Glass Fiber Reinforced Polymer (GFRP) jacketing proved to be an effective method for rehabilitating the joint. This technique maintained the concrete's integrity by confinement, leading to a significant improvement in both ductility and load-carrying capacity for the repaired joint [3].

A study explores the susceptibility of beam-column joints in reinforced concrete structures to lateral loads and presents a finite element model for simulating their seismic behavior. Retrofitting existing structures, a significant challenge in contemporary civil engineering, is addressed through jacketing to improve the strength and stiffness of exterior beam-column joints. An analytical model is suggested to estimate shear capacity, enhanced by carbon fiber-reinforced polymer (CFRP). Through cyclic loading of two specimens, one without reinforcement and another with CFRP strengthening, the study demonstrates that CFRP reinforcement enhances structural stiffness, strength, and energy dissipation capacity, providing an effective strategy for rehabilitation [11]. This study focuses on assessing the performance of beam-column joints subjected to cyclic loads, employing a modified reinforcement technique at the junction. The shear strengthening can be done by using a modified reinforcement technique such as using GFRP for RC beam column joints. The primary objective of this study is to conduct numerical analysis on beam-column joints subjected to cyclic loading, particularly exploring scenarios where the beam exhibits weakness in shear. To address this vulnerability, the study aims to enhance shear performance in RC beam-column joints by employing GFRP. The numerical investigation will be conducted using ANSYS Mechanical APDL, allowing for a comprehensive assessment of the structural behavior of beam-column joints under cyclic loading conditions with the added strength provided by GFRP.

The ANSYS software, renowned for its powerful features, prominently features the ANSYS Parametric Design Language (APDL). This software empowers users to define various critical aspects of a model, including geometry, material properties, and loads, through parameters. The flexibility provided by APDL allows for straightforward modifications and the solution of various model variations by simply adjusting parameter values and rerunning the model. ANSYS, with its parametric capabilities, emerges as a versatile tool for engineering analysis, optimization, root cause analysis, and the design of innovative systems and technologies. APDL further extends its utility by supporting the creation and execution of macros, enabling users to run them as ANSYS commands, manipulate parameter arrays, and implement logical operations. Additionally, ANSYS accommodates both steady-state and time-dependent analyses, covering static analyses without inertia effects and dynamic analyses where inertia effects play a significant role. The software's capability extends to various types of static

analyses, including single-step and multistep approaches, allowing for the application or removal of different loads in each step. In a single run, multistep analyses in ANSYS facilitate solving multiple load combinations and allow for the gradual application of loads in nonlinear analyses, where time is crucial, and the consideration of mass effects is not neglected. ANSYS further supports nonlinear transient dynamic analysis, capturing time-dependent system responses to changing loads and nonlinearities [12].

The examination of numerical analysis in reinforced RC structures, particularly focusing on beam-column joints subjected to cyclic loading, finds itself at the intersection of established design principles and advanced testing methodologies. Guided by the Indian standards IS 456-2000 (Plain and Reinforced Concrete - Code of Practice) [13] and IS 13920-2016 (Ductile Design and Detailing of Reinforced Concrete Structures Subjected to Seismic Forces - Code of Practice) [14], this investigation establishes a sturdy foundation. Employing the design aids from SP-16 (Design Aids For Reinforced Concrete to IS: 456-1978) [15] for reinforced concrete and adhering to ductile detailing provisions, this investigation explores the delicate balance between material properties and loading conditions, aligning with the provisions of IS 456-2000. Acknowledging the behavior of beam-column joints to cyclic loading, ductile detailing is prioritized in potential stress zones, ensuring ample reinforcement confinement and appropriate design strength. In regions prone to seismic activity, the IS 13920-2016, integrating seismic factors into the numerical investigations applied for the seismic design category of the project site. Additionally, this study integrates cyclic load testing methodologies outlined in ASTM E2126–11 (Standard Test Methods for Cyclic (Reversed) Load Test for Shear Resistance of Vertical Elements of the Lateral Force Resisting Systems for Buildings) [16] to simulate and evaluate the behavior of beam-column joints under cyclic displacement. In summary, these codes and standards ensure that RC structures are designed, detailed, and tested in a manner that prioritizes safety, durability, and the ability to withstand various forces, including seismic events and cyclic loading. Adhering to these codes helps this study to meet standards and regulatory requirements, contributing to the overall reliability and resilience of structures.

The numerical examination of RC beam-column joints under cyclic loading incorporates essential codes to ensure improved structural performance. SP-16 with IS 456-2000 supports effective and secure design. IS 456-2000 provides standard design provisions for beam and column designs, assuring structural integrity. IS 13920-2016 ensures ductile detailing and joint design, particularly crucial in seismic zones. Additionally, ASTM E2126–11 provides standardized procedures for cyclic load testing, specifically addressing shear resistance in beam-column joints. The RC beam column joints are designed following these codal provisions. The study focuses on the numerical investigation of RC beam-column joints subjected to cyclic loading, specifically exploring scenarios where the beam exhibits weakness in shear by reducing shear reinforcement in beams. The shear performance of beams weak in shear within RC beam-column joints is enhanced by the application of GFRP composites. To achieve this, numerical investigation employs the powerful capabilities of ANSYS Mechanical APDL. The methodology aims to assess the structural behavior of these beam-column joints under cyclic loading conditions, with a particular emphasis on the improvements achieved through GFRP-enhanced shear strength. The use of these materials supports environmental sustainability by reducing environmental harm [17–20]. This approach combines numerical analysis, material reinforcement, and advanced simulation techniques to provide insights into the performance enhancement of RC beam-column joints, under cyclic loading.

RESEARCH SIGNIFICANCE

The extensive research conducted on BCJs over the past decades has significantly contributed to understanding their behavior. However, despite the prevalence of such studies, structural failures persist, prompting the need for further investigation. This study aims to address this challenge by focusing on the strong column-weak beam concept, crucial for preventing localized beam failures that could lead to progressive collapses. By analyzing the ductility of joints compared to conventional methods and exploring shear reinforcement reduction, this research seeks to enhance structural

resilience. Moreover, adhering to updated design codes ensures alignment with contemporary standards, while incorporating cyclic loading enables realistic simulation of dynamic structural responses. This study also examines the potential of GFRP for enhancing the shear capacity of beams, thereby broadening the investigation to include innovative strengthening techniques aimed at improving structural performance and resilience.

DESCRIPTION OF RC BCJ MODELS

The codes provided, such as BWSCL, BWSRL, BWSCM, BWSRM, BWSCS, and BWSRS, are likely identifiers for different types of BCJ specimens used in researching shear strength characteristics. BWS indicates Beam Weak in Shear in BCJ specimen. These codes are accompanied by numerical values (100, 70, 50) indicating the percentage of shear reinforcement within the beams, where higher percentages signify increased reinforcement. L, M, and S indicate large, Medium, and Small respectively for full scale, $^2/_3$ scale and $^1/_3$ scale specimens. Additionally, terms like "Full scale," "$^2/_3$ scale," and "$^1/_3$ scale" specify the size of the BCJ specimens, ranging from actual dimensions to smaller fractions. These classifications imply a thorough examination of beam behavior under varied levels of shear reinforcement and testing conditions, with the aim of advancing understanding in structural performance and guiding design practices. The description of BCJ specimens is shown in the Table 1. The dimensions of specimens of varying scales are given in Table 2. Table 3 shows the longitudinal and transverse reinforcement details of beams in BCJ Specimens of all scales. Figure 1 depicts the details of BCJ specimens.

Table 1. Designation of Specimens with description

Specimen Name	Description
BWSCL100	Beam weak in shear controlled full scale with 100% shear reinforcement
BWSCL70	Beam weak in shear controlled full scale with 70% shear reinforcement
BWSCL50	Beam weak in shear controlled full scale with 50% shear reinforcement
BWSRL100	Beam weak in shear Retrofitted full scale with 100% shear reinforcement
BWSRL70	Beam weak in shear Retrofitted full scale with 70% shear reinforcement
BWSRL50	Beam weak in shear Retrofitted full scale with 50% shear reinforcement
BWSCM100	Beam weak in shear controlled $^2/_3$ scale with 100% shear reinforcement
BWSCM70	Beam weak in shear controlled $^2/_3$ scale with 70% shear reinforcement
BWSCM50	Beam weak in shear controlled $^2/_3$ scale with 50% shear reinforcement
BWSRM100	Beam weak in shear Retrofitted $^2/_3$ scale with 100% shear reinforcement
BWSRM70	Beam weak in shear Retrofitted $^2/_3$ scale with 70% shear reinforcement
BWSRM50	Beam weak in shear Retrofitted $^2/_3$ scale with 50% shear reinforcement
BWSCS100	Beam weak in shear controlled $^1/_3$ scale with 100% shear reinforcement
BWSCS70	Beam weak in shear controlled $^1/_3$ scale with 70% shear reinforcement
BWSCS50	Beam weak in shear controlled $^1/_3$ scale with 50% shear reinforcement
BWSRS100	Beam weak in shear Retrofitted $^1/_3$ l scale with 100% shear reinforcement
BWSRS70	Beam weak in shear Retrofitted $^1/_3$ scale with 70% shear reinforcement
BWSRS50	Beam weak in shear Retrofitted $^1/_3$ scale with 50% shear reinforcement

Table 2. Dimensions of the specimens.

Column Dimensions				Beam Dimensions		
Specimen Name	***Length (mm)***	***Width (mm)***	***Depth (mm)***	***Length (mm)***	***Width (mm)***	***Depth (mm)***
BWSCL100	3000	450	300	1500	300	300
BWSCL70						
BWSCL50						
BWSRL100						
BWSRL70						
BWSRL50						
BWSCM100	2000	300	200	1000	200	200

BWSCM70						
BWSCM50						
BWSRM100						
BWSRM70						
BWSRM50						
BWSCS100	1000	150	100	500	100	100
BWSCS70						
BWSCS50						
BWSRS100						
BWSRS70						
BWSRS50						

Table 3. Reinforcement Details of beams in BCJ specimens.

		Longitudinal Reinforcement		Transverse Reinforcement	
S.N.	***Specimen Designation***	***No. of Bars and Diameter***	***A_{st} (mm^2)***	***No. of Bars and Diameter***	***A_{st} (mm^2)***
1	BWSCS100	Top r/f 4-16 mm Bottom r/f 2-12 mm	804.25 226.19	15-8Ø	753.98
2	BWSRS100				
3	BWSCL70			11-8Ø	552.92
4	BWSRS70				
5	BWSCS50			7-8Ø	351.86
6	BWSRL50				
7	BWSCS100	Top r/f 3-16 mm Bottom r/f 2-12 mm	603.18 226.19	10-8Ø	502.65
8	BWSRS100				
9	BWSCS70			7-8Ø	351.86
10	BWSRS70				
11	BWSCS50			5-8Ø	231.32
12	BWSRS50				
13	BWSCS100	Top r/f 2-16 mm Bottom r/f 2-12 mm	402.12 226.19	10-6Ø	282.74
14	BWSRS100				
15	BWSCS70			7-6Ø	197.92
16	BWSRS70				
17	BWSCS50			5-6Ø	141.37
18	BWSRS50				

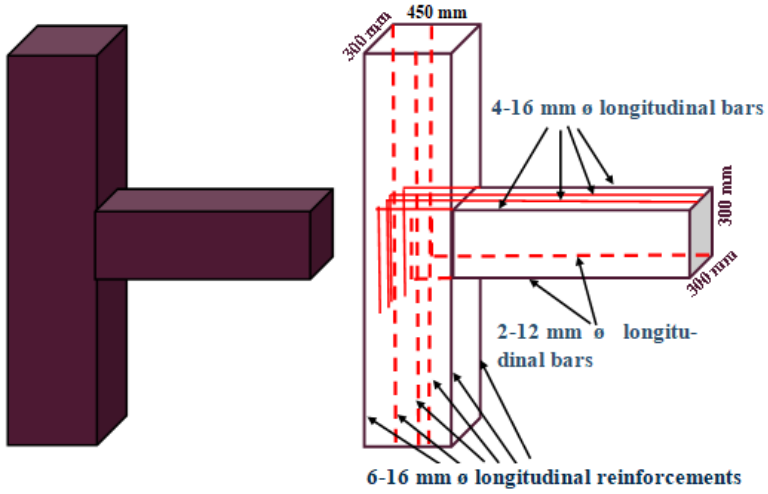

Figure 1. Detailing of BCJ.

In Table 4, the reinforcement detailing of columns in BCJ specimens is presented. This table outlines the specific configuration and arrangement of reinforcement within the columns.

Table 4. Reinforcement Detailing of Column in BCJ specimens.

		Longitudinal Reinforcement		Transverse Reinforcement	
S.N.	***Specimen Designation***	***No. of Bars and Diameter***	***A_{st} (mm^2)***	***No. of Bars and Diameter***	***A_{st} (mm^2)***
1	BWSCL100	6-16Ø	1206.37	20-8Ø	1005.3
2	BWSCL70				
3	BWSCL50				
4	BWSRL100				
5	BWSRL70				
6	BWSRL50				
7	BWSCM100			15-8Ø	754
8	BWSCM70				
9	BWSCM50				
10	BWSRM100				
11	BWSRM70				
12	BWSRM50				
13	BWSCS100			10-6Ø	282.74
14	BWSCS70				
15	BWSCS50				
16	BWSRS100				
17	BWSRS70				
18	BWSRS50				

Table 5 outlines the material characteristics of concrete and steel utilized in Numerical investigation. Concrete is represented by the Solid65 element type, chosen for its capacity to depict nonlinear material traits such as cracking and crushing. Conversely, steel is denoted by the Link 180 element type, which accurately models the linear elastic behavior of steel components.

Table 5. Material properties of Concrete and Steel.

Materials	**Element type**
Note: Preference	Structural
For concrete	Solid65
For steel	Link 180
	For concrete and steel

Materials	***Young's Modulus(N/mm^2)***	***Poisson's Ratio***
Concrete	25000	0.15
Steel	200000	0.3
	For Fe500 Steel	

Properties	Values
Yield Stress	500 N/mm^2
Tangent Modulus	20

Table 6 presents the material characteristics of GFRP. These properties are vital for understanding the behavior and performance of GFRP in structural applications. Detailed information on factors such as tensile strength, modulus of elasticity, and density allows for accurate analysis and design of GFRP

components. Such data aids engineers in optimizing the use of GFRP materials for lightweight, durable, and corrosion-resistant structural solutions.

Table 6. Material Properties of GFRP (ANSYS WORKBENCH DATA).

Property	Value	Unit
1. Density	2000	kg/m^3
2. Orthotropic Elasticity		
A. Young's Modulus X direction	4.5E+10	Pa
B. Young's Modulus Y direction	1E+10	Pa
C. Young's Modulus Z direction	1E+10	Pa
D. Poisson's Ratio XY	0.3	---
E. Poisson's Ratio YZ	0.4	---
F. Poisson's Ratio XZ	0.3	---
G. Shear Modulus XY	5E+09	Pa
H. Shear Modulus XY	3.846E+09	Pa
I. Shear Modulus XY	5E+09	Pa

Table 7 provides the amplitudes of the reversed cycles according to Test Method B as outlined in the ASTM 2015 standard. The table shows cyclic loading protocol used for this numerical investigation on BCJ specimens for beam weak in shear under cyclic load.

Table 7. Test Method B-Amplitudes of the Reversed Cycles (ASTM 2015).

Pattern	Load Step	Minimum Number of Cycles	Amplitudes, (D_m)
1	1	1	0.0125
	2	1	0.025
	3	1	0.05
	4	1	0.075
	5	1	0.1
2	6	3	0.2
	7	3	0.4
	8	3	0.6
	9	3	0.8
	10	3	1
	11	3	1.2
			Additional increment of 20% (until specimen failure)

Figure 2 displays the meshed view and discretization of reinforcements of various specimens utilized in this investigation. These figures illustrate the longitudinal and shear reinforcements and discretization process for different specimens, including BWSCL100, BWSCL70, BWSCL50, BWSCM100, BWSCM70, BWSCM50, BWSCS100, BWSCS70, and BWSCS50. Each figure provides a detailed representation of the reinforcement layout and meshing technique employed for the respective specimen, offering insights into the structural configuration utilized in the study. The meshed views illustrate how the reinforcement elements are distributed spatially within the specimens, whereas the discretization diagrams provide insight into the finite element modeling (FEM) method utilized to replicate the behavior of the structures being studied.

Figures 3(a) to 3(f) display solid and meshed perspectives of specimens at various scales, offering insights into the structural layouts of BWSCL100, BWSCM100, and BWSCS100. Solid views provide a detailed representation of each specimen's geometry and material distribution, while meshed views illustrate how structures are discretized into finite elements for computational analysis. This

presentation method facilitates a comprehensive understanding of specimen geometry and meshing strategies, assisting researchers in interpreting structural responses and performance under diverse loading scenarios. Figure 3 presents both solid and meshed views of specimens across different scales.

Figure 4 depicts the use of GFRP wrapping on different specimens, offering solid and meshed perspectives for each scenario. In Figures. 4(a), (c), and (e), solid views depict the physical application of GFRP wrapping on BWSCL100, BWSCL70, and BWSCL50 specimens, respectively, providing insights into their layout and positioning. Conversely, Figures 4(b), (d), and (f) present meshed views, showcasing how the GFRP wrapping is discretized into finite elements for computational analysis. These views elucidate the meshing method utilized to simulate the behavior of GFRP wrapping under diverse loading conditions. The combination of solid and meshed views aids comprehension of GFRP wrapping application and structural behavior across various specimens, facilitating assessment of its efficacy in improving the performance and longevity of reinforced concrete components.

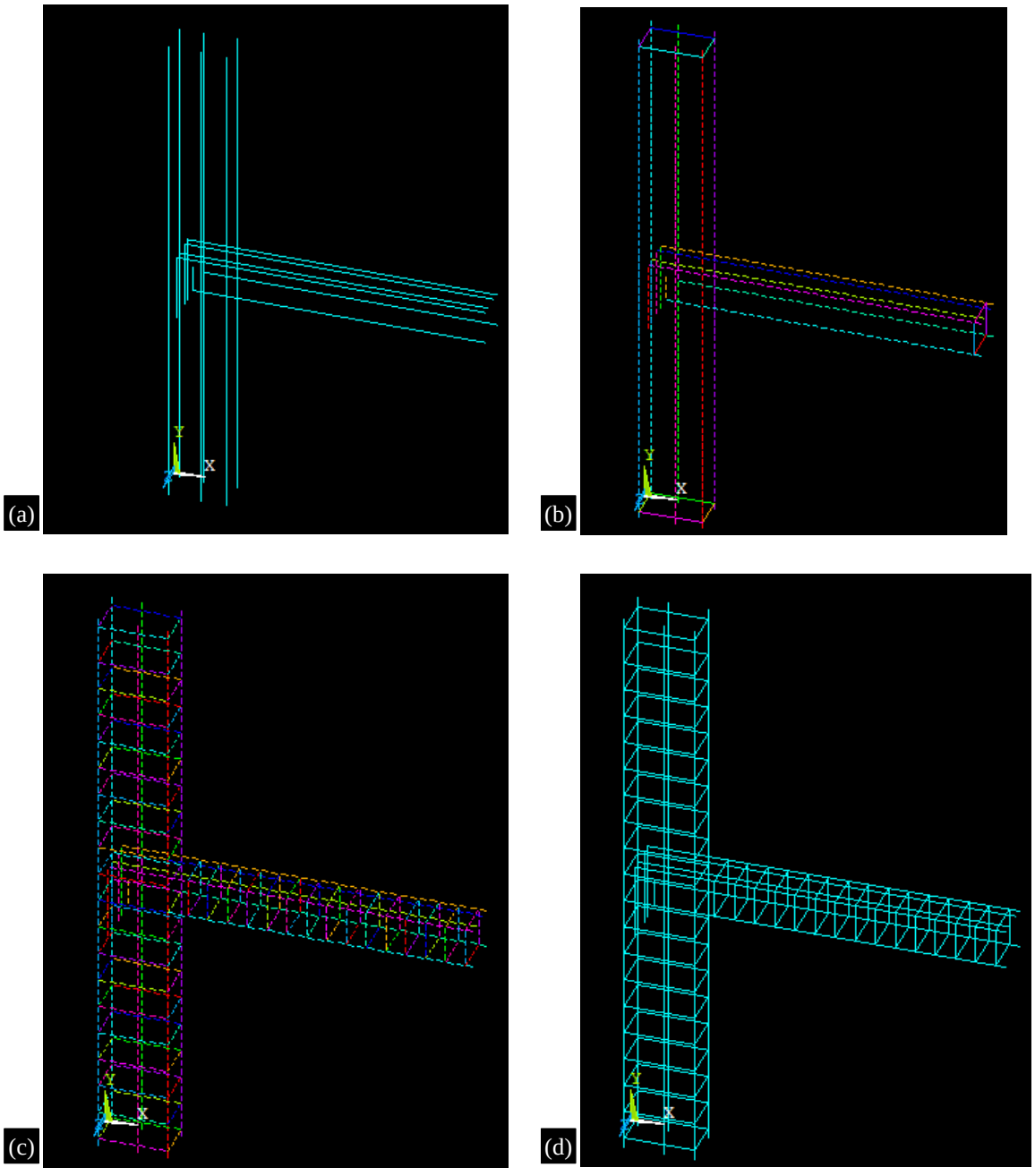

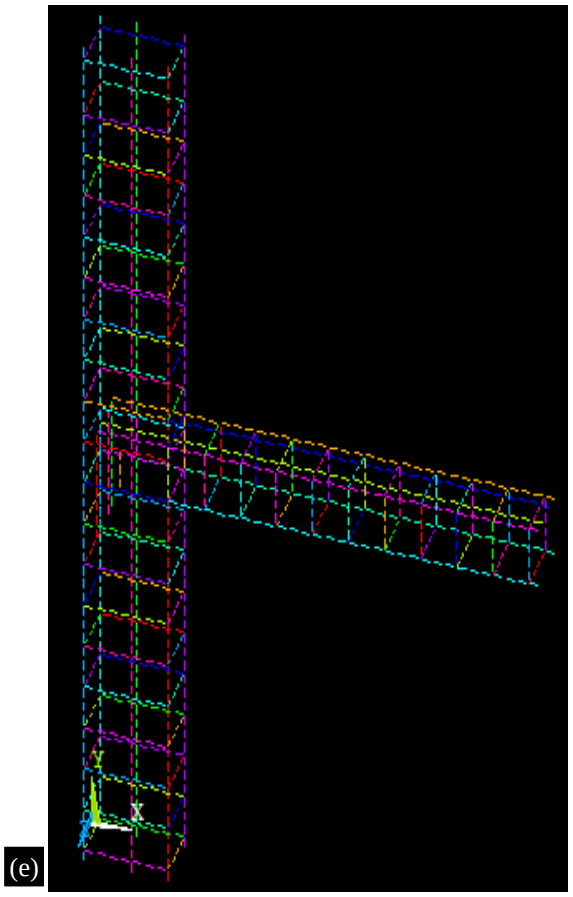
(e)

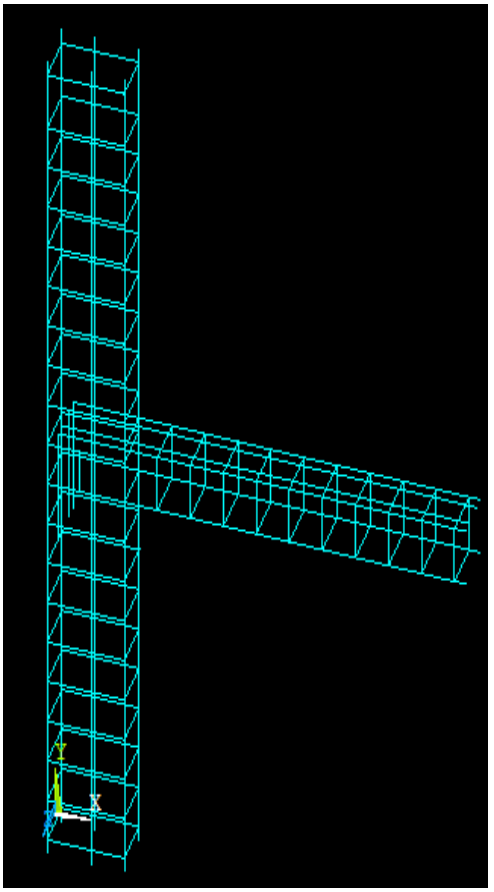
(f)

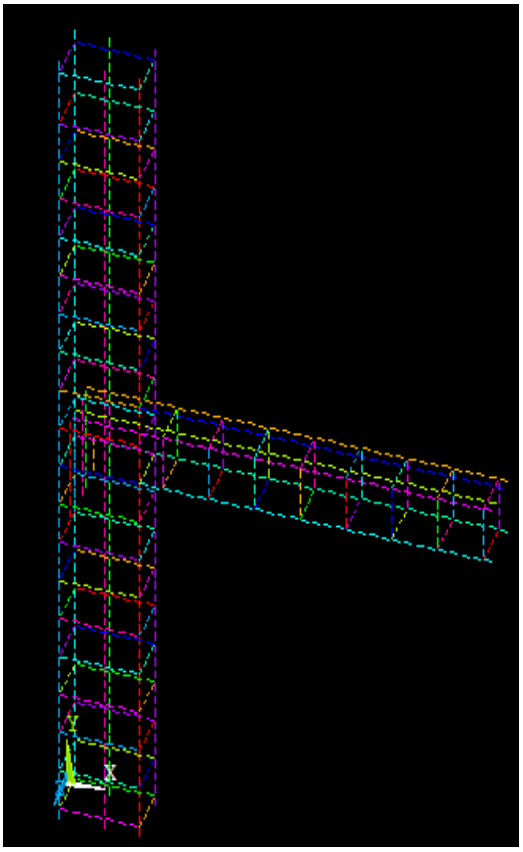
(g)

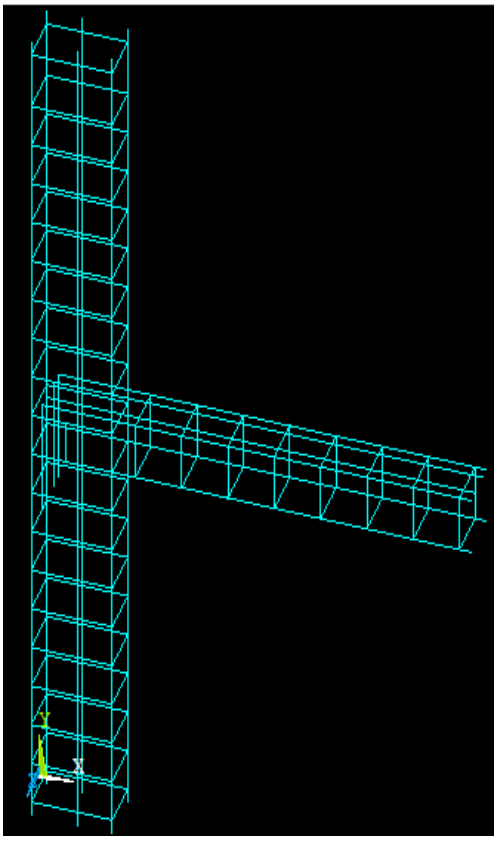
(h)

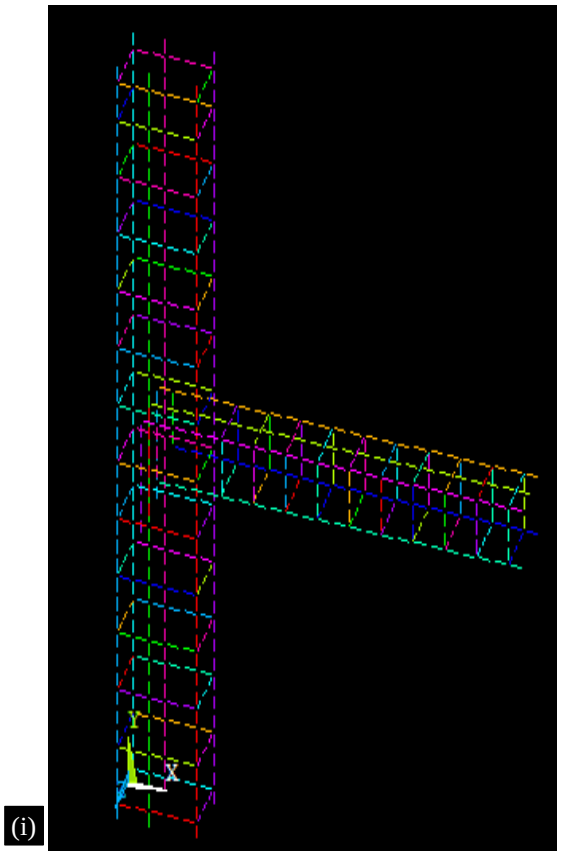

(i)

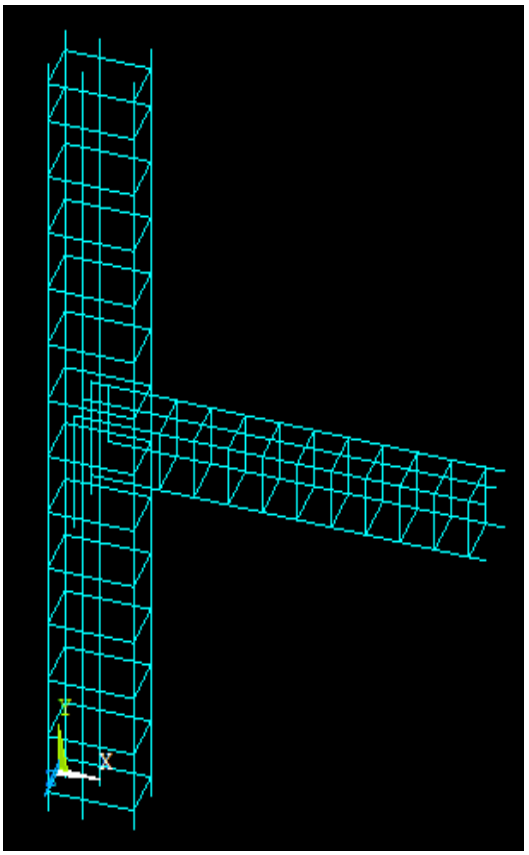

(j)

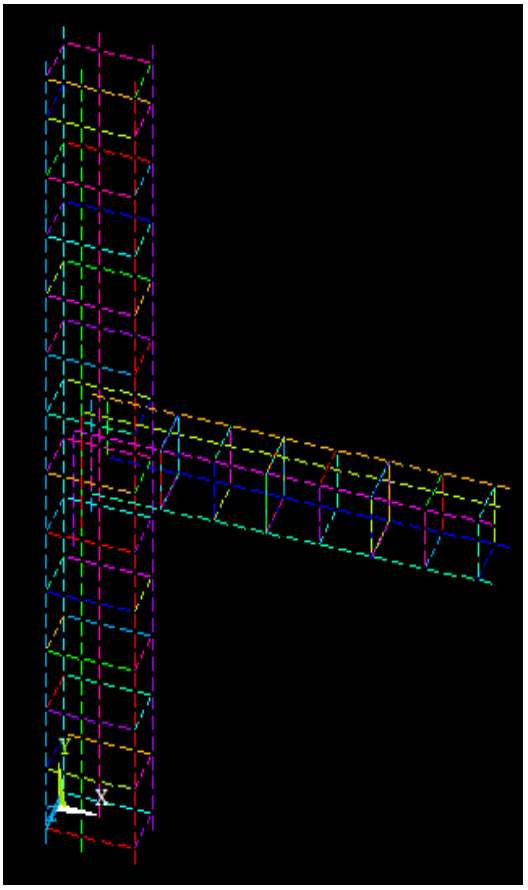

(k)

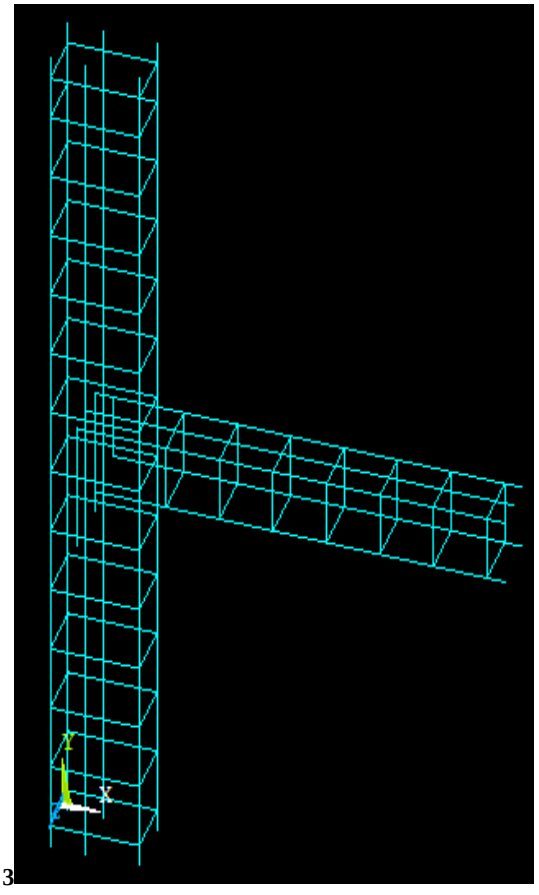

(l)

3

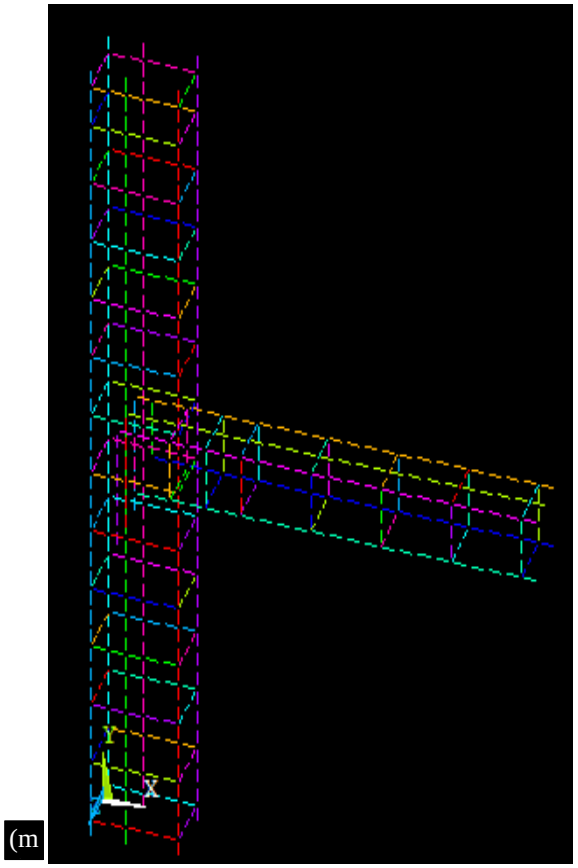

(m)

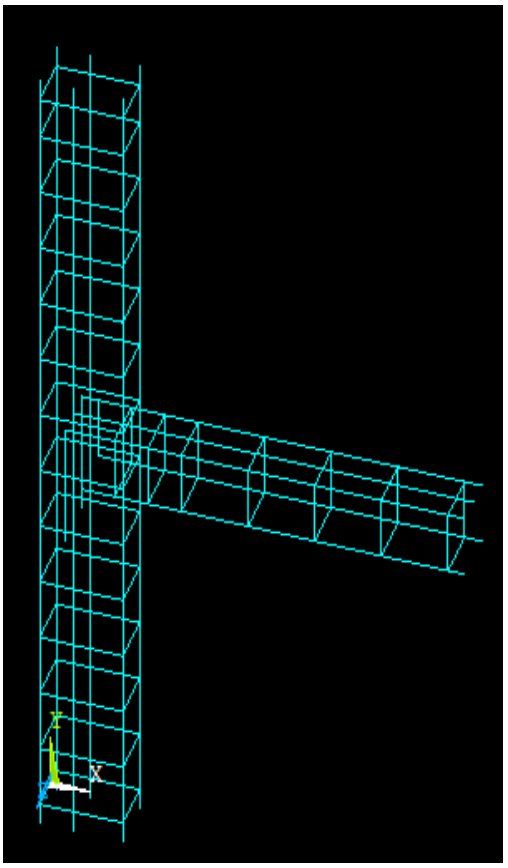

(n)

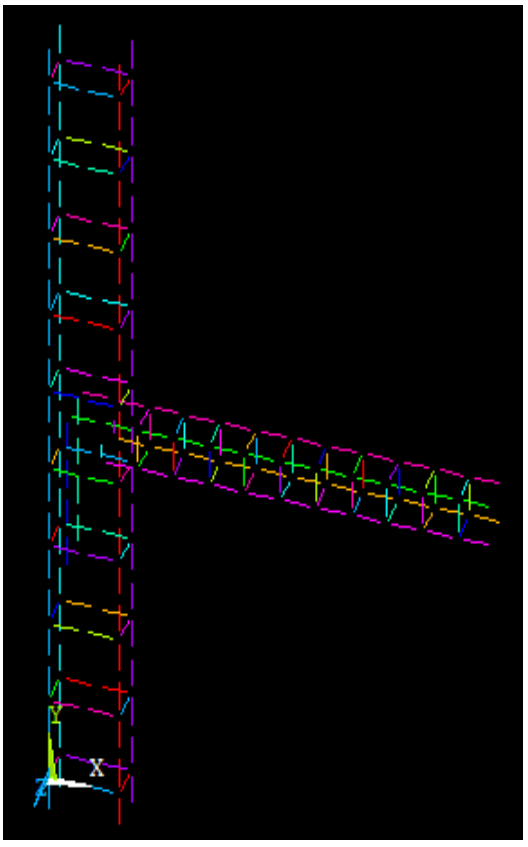

(o)

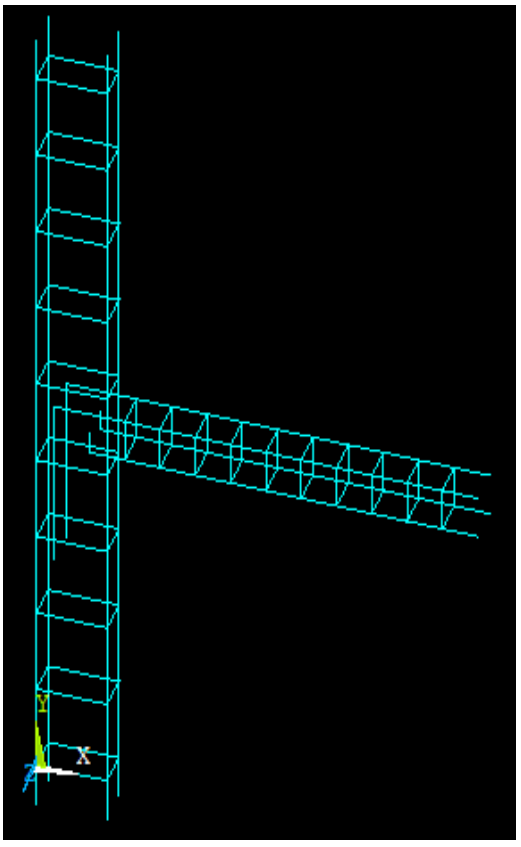

(p)

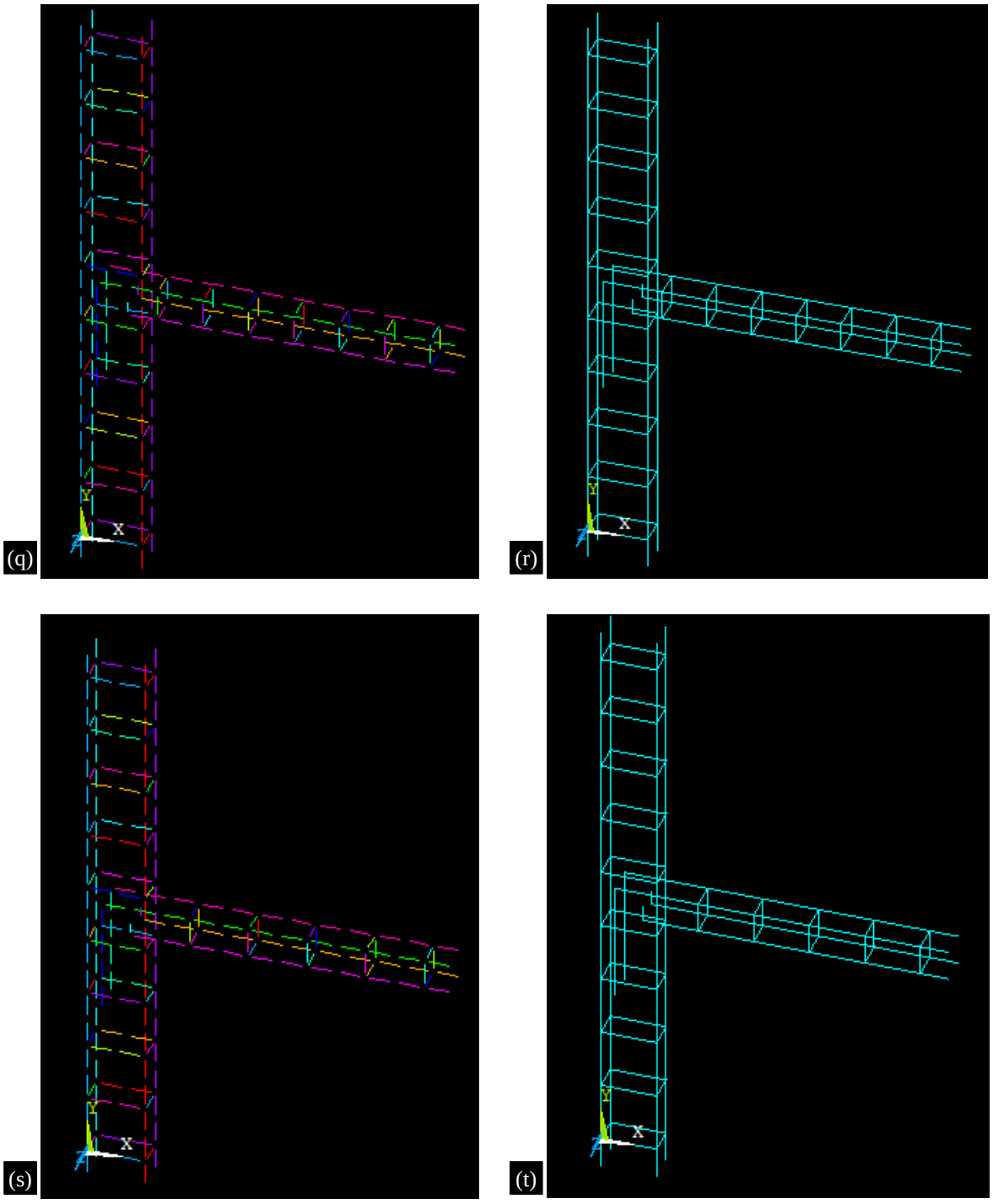

Figure 2. Meshed view and Discretization of different specimens used for this investigation. (a) Meshed view of longitudinal reinforcement. (b) Discretization of longitudinal reinforcement. (c) Meshed view of Reinforcements of BWSCL100 (d) Meshed view of reinforcement of BWSCL100 (e) Discretization of reinforcements of BWSCL70 (f) Meshed View of reinforcements of BWSCL70 (g) Discretization of reinforcements of BWSCL50 (h) Meshed view of reinforcements of BWSCL50 (i) Discretization of reinforcements of BWSCM100 (j) Meshed view of reinforcements of BWSCM100 (k) Discretization of reinforcements of BWSCM70 (l) Meshed view of reinforcements of BWSCM70 (m) Discretization of reinforcements of BWSCM50 (n) Meshed view of reinforcements of BWSCM50 (o) Discretization of reinforcements of BWSCS100 (p) Meshed view of reinforcements of BWSCS100 (q) Discretization of reinforcements of BWSCS70 (r) Meshed view of reinforcements of BWSCS70 (s) Meshed view of reinforcements of BWSCS50 (t) Meshed view of reinforcements of BWSCS50.

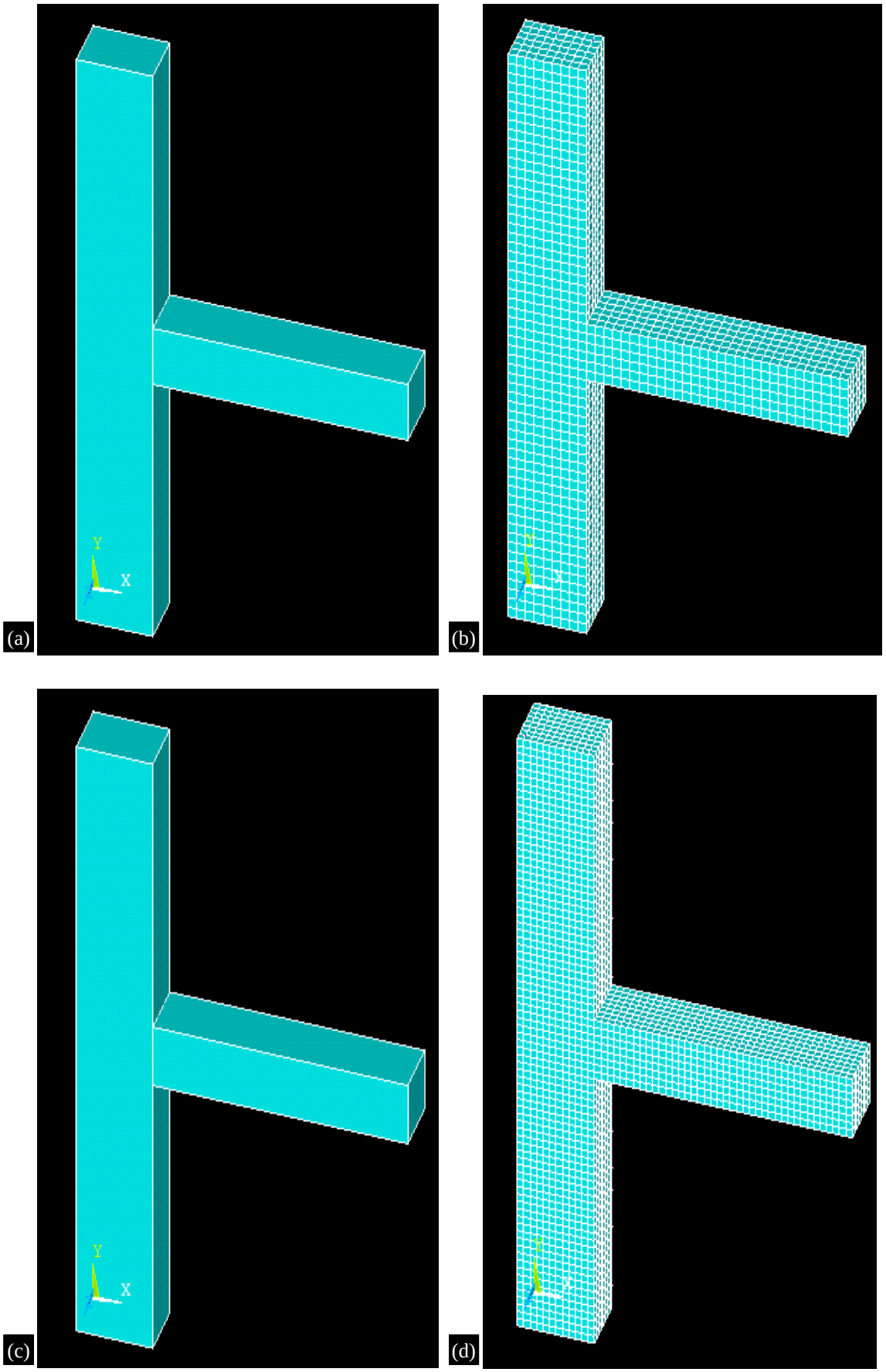

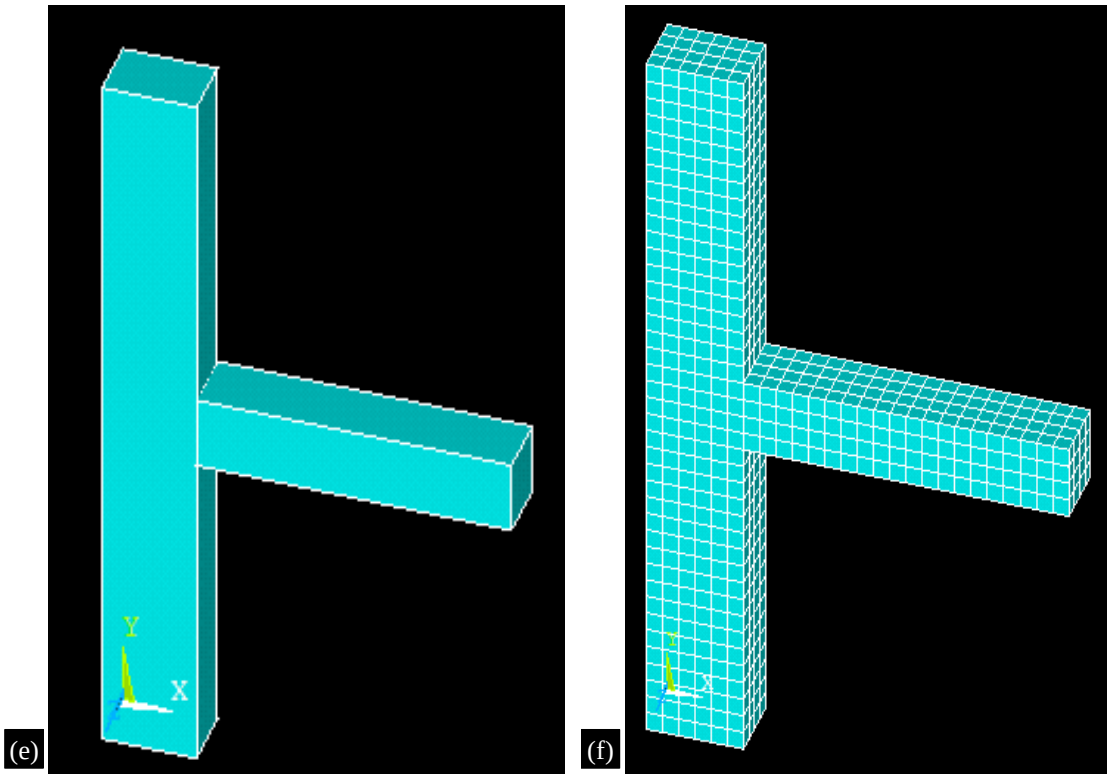

Figure 3. Solid and Meshed view of specimens of varying scale. (a) Solid view of BWSCL100 (b) Meshed view of BWSCL100 (c) Solid view of BWSCM100 (d) Meshed view of BWSCM100 (e) Solid view of BWSCS100 (f) Meshed view of BWSCS100.

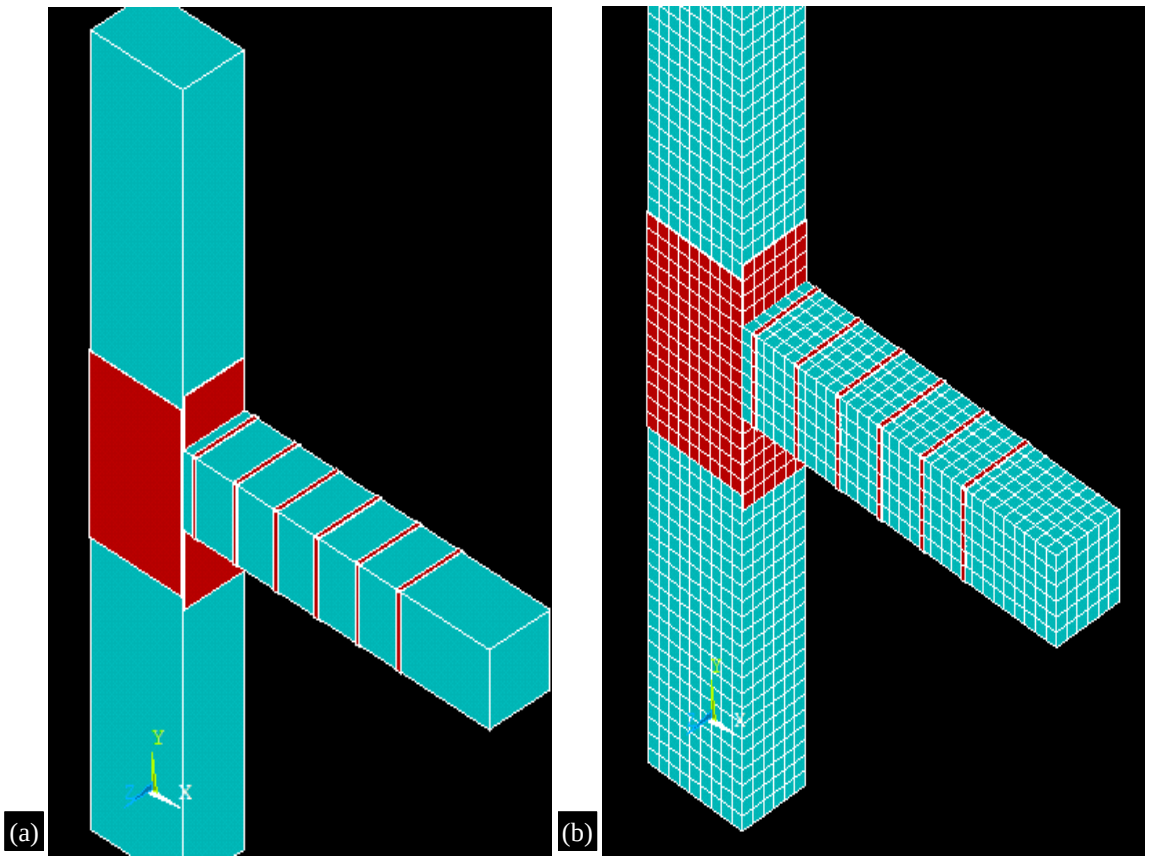

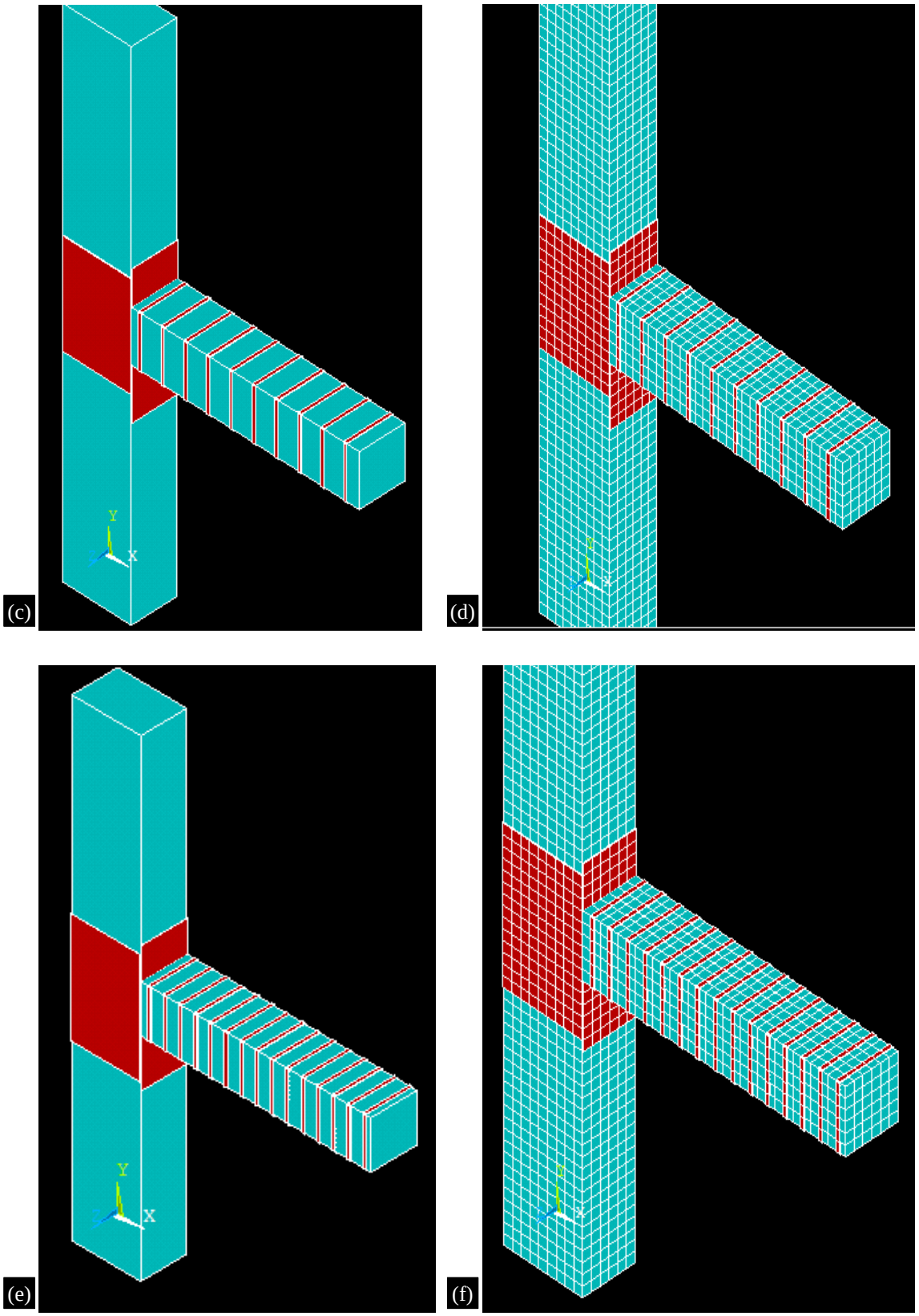

Figure 4. GFRP wrapping on different specimens. (a) GFRP wrapping for BWSCL100(solid view) (b) GFRP wrapping for BWSCL100(meshed view) (c): GFRP wrapping for BWSCL70(solid view) (d) GFRP wrapping for BWSCL70(Meshed view) (e) GFRP wrapping for BWSCL50(solid view) (f): GFRP wrapping for BWSCL50(Meshed view).

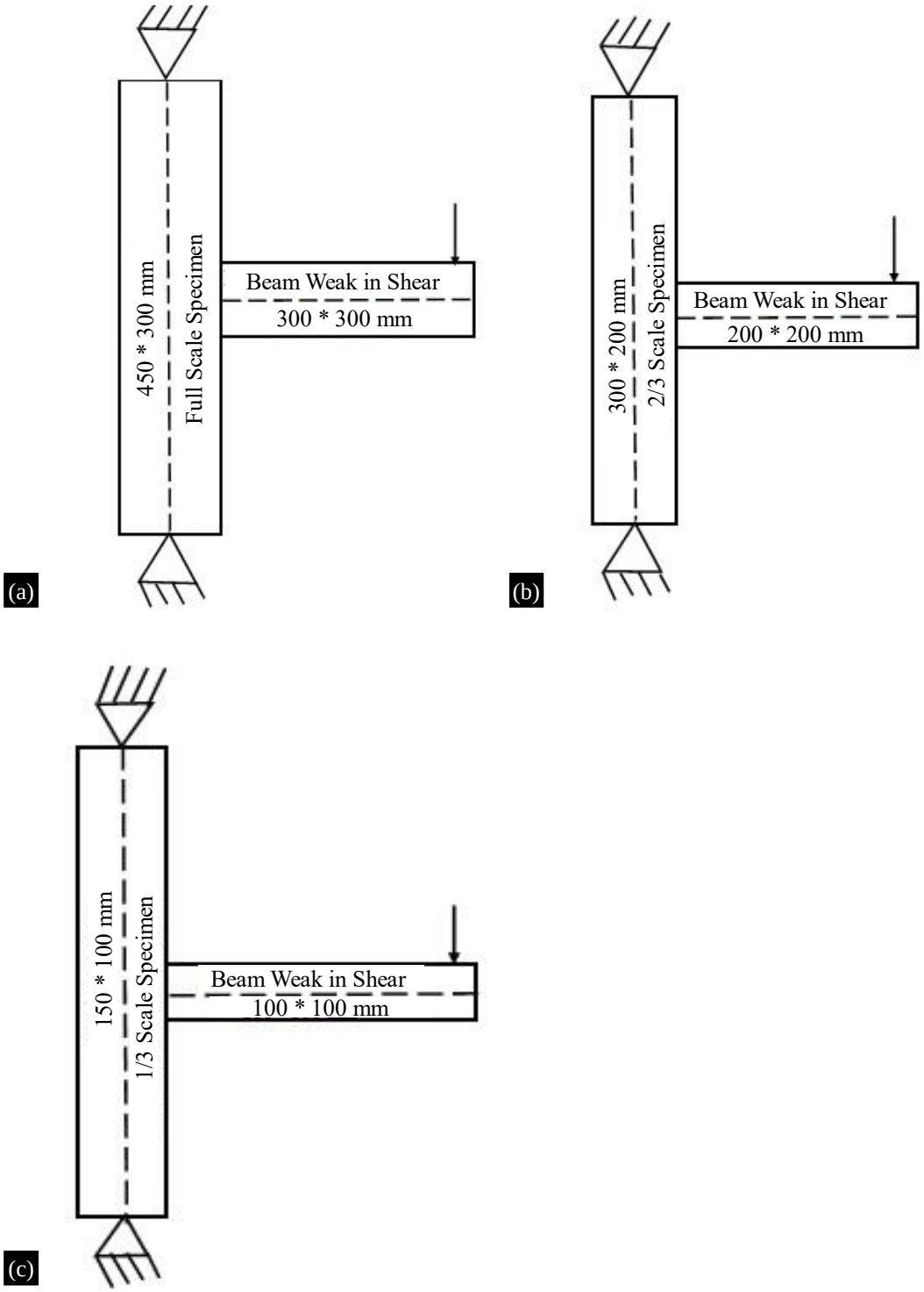

Figure **5**. Loading setup for specimens of varying scale. (a) Loading setup for Full scale specimens. (b) Loading setup for $^{2}/_{3}$ scale specimens. (c) Loading Setup for $^{1}/_{3}$ scale specimens.

RESULTS AND DISCUSSIONS

Figure 6 illustrates the displaced structure of BWSCL specimens in downward and upward directions. Additionally, it displays the displaced structure of BWSRL specimens in both directions. These visual representations provide significant insights into the structural behavior of the specimens under different loading conditions, aiding in the assessment of their performance and the effectiveness of retrofitting techniques in improving their strength and stability.

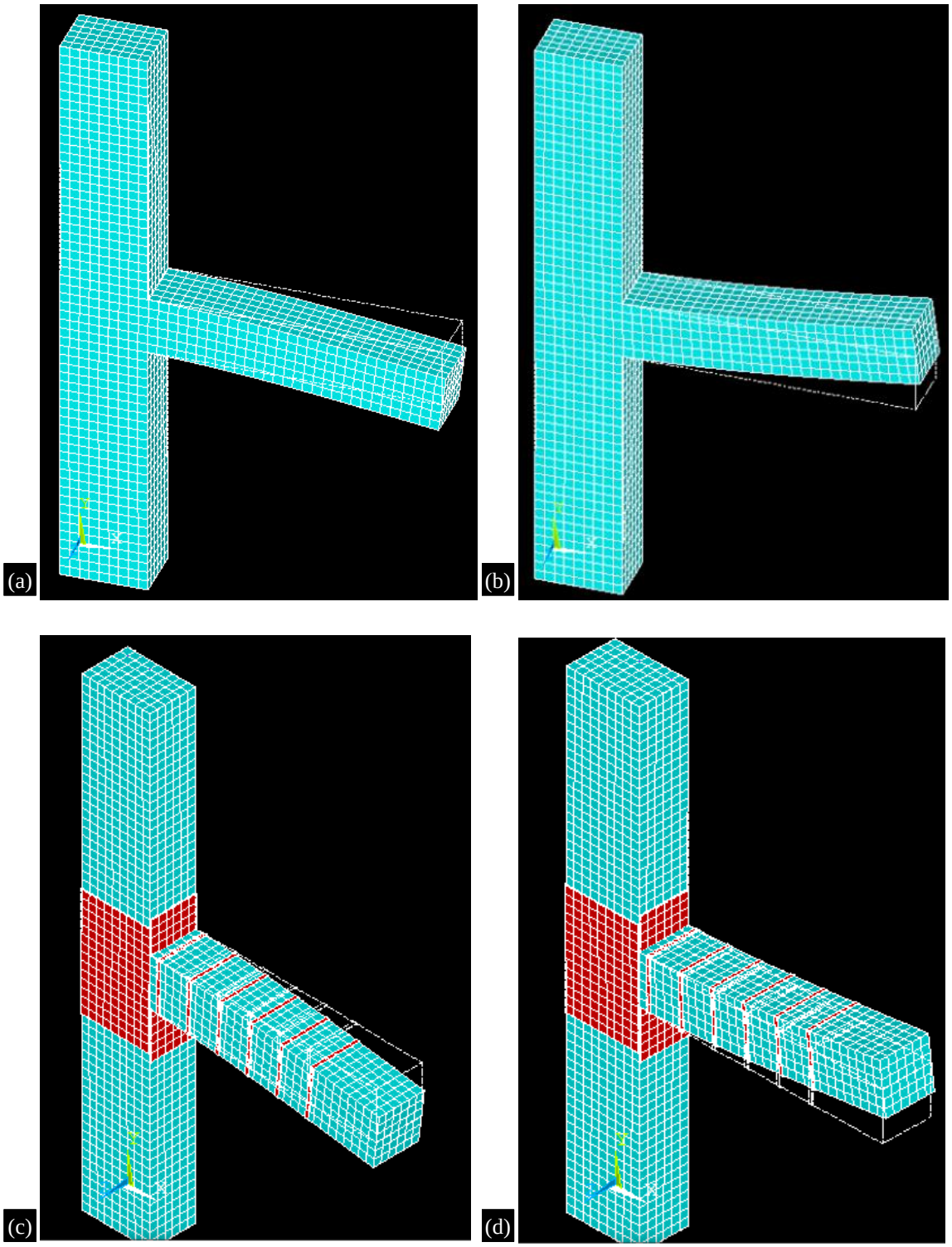

Figure 6. (a) Displaced structure of BWSCL SPECIMENS in Downward Direction (b) Displaced structure of BWSCL SPECIMENS in Upward Direction (c) Displaced Structure of BWSRL Specimens in Downward Direction. (d) Displaced Structure of BWSRL Specimens in Upward Direction.

Figure 7 displays the crack patterns observed in both controlled (BWSCL100) and retrofitted (BWSRL100) specimens. In Figure 7(a), the crack pattern for BWSCL100 is depicted, while Figure 7(b) displays the crack pattern for BWSRL100. These visual representations provide insight into the differences in crack formation and distribution between the controlled and retrofitted specimens,

offering valuable information for assessing the effectiveness of the retrofitting technique. The retrofitting helped to improve the shear behavior of beams and it helped to make the joint strong enough to resist the cyclic load up to a certain limit the difference can be observed in the given Figure 7 as there is improvement in the BWSRL100 specimen compared to BWSCL100 Specimen.

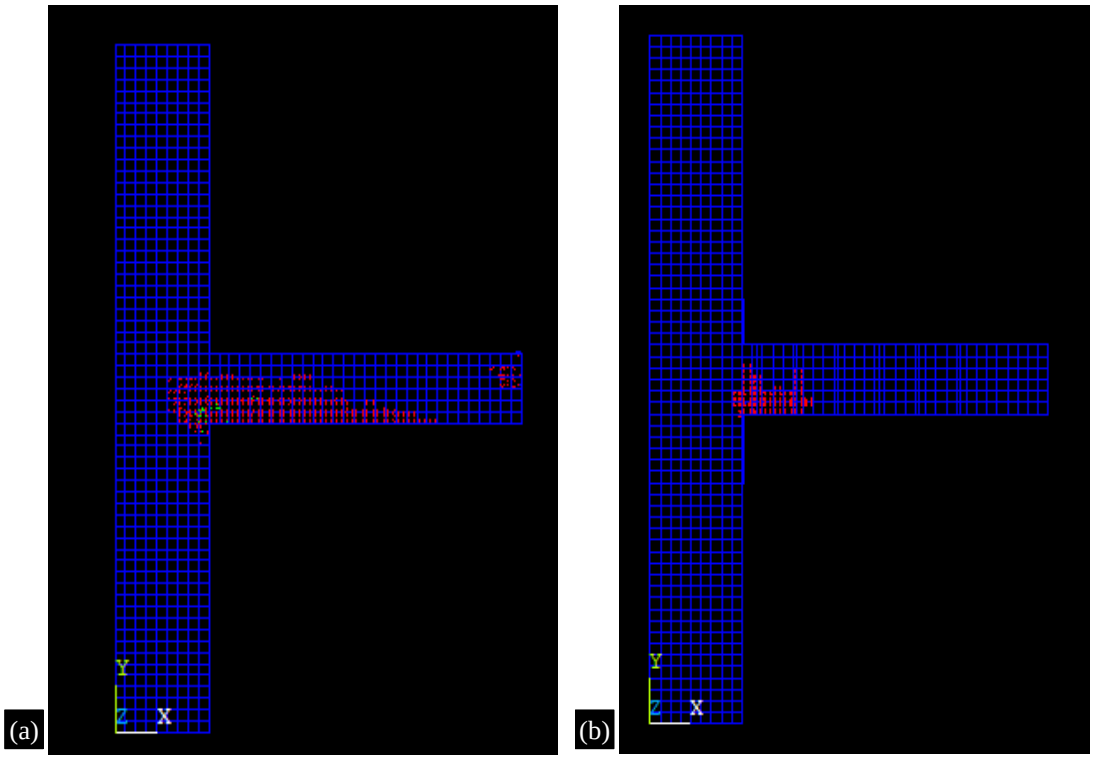

Figure 7. Crack Patterns for Controlled and Retrofitted Specimens (BWSCL100 AND BWSRL100). (a) Crack Pattern for BWSCL100 (b) Crack Pattern for BWSRL100.

Figures 8–10 extensively explore the relation between lateral load and displacement across a diverse scale of specimens with different shear reinforcement percentages in beam. These figures serve as visual representations of how structures respond to lateral forces, showcasing significant insights into their behavior and performance under cyclic loading circumstances. Figure 8 presents the lateral load versus displacement graphs for specimens BWSCL100, BWSRL100, BWSCL70, BWSRL70, BWSCL50, and BWSRL50, displayed in panels 8(a) to 8(f) respectively. Similarly, Figure 9 illustrates this relationship for specimens BWSCM100, BWSRM100, BWSCM70, BWSRM70, BWSCM50, and BWSRM50, showcased in 9(a) 9(f) correspondingly. Additionally, Figure 10 explores this correlation for specimens BWSCS100, BWSSRS100, BWSCS70, BWSRS70, BWSCS50, and BWSRS50, depicted in Figure 10(a) to 10(f) respectively. These figures are important for analyzing and assessing how structures respond to lateral loads, to evaluate factors like stiffness, strength, and ductility across different specimen sizes. By comparing the lateral load versus displacement curves of controlled and retrofitted specimens, significant information can be gleaned regarding the efficacy of retrofitting methods in enhancing structural performance and resilience. Moreover, these plots offer significant data for validating analytical models and finite element simulations, ensuring the accuracy and reliability of predictive tools used in structural engineering. The observed trends and patterns in lateral load-displacement behavior contribute to a deeper understanding of structural response mechanisms, guiding the development of more effective and reliable design approaches. We can observe the improvement in the structural behavior in retrofitted specimens. Shear behavior is improved with GFRP wrapping and it is observed from the plots clearly. Hence, these plots show that the retrofitting on the beams weak in shear has gained the shear strength and joints also get improved structural capacity providing a complete solution to withstand the cyclic load up to a certain design limit.

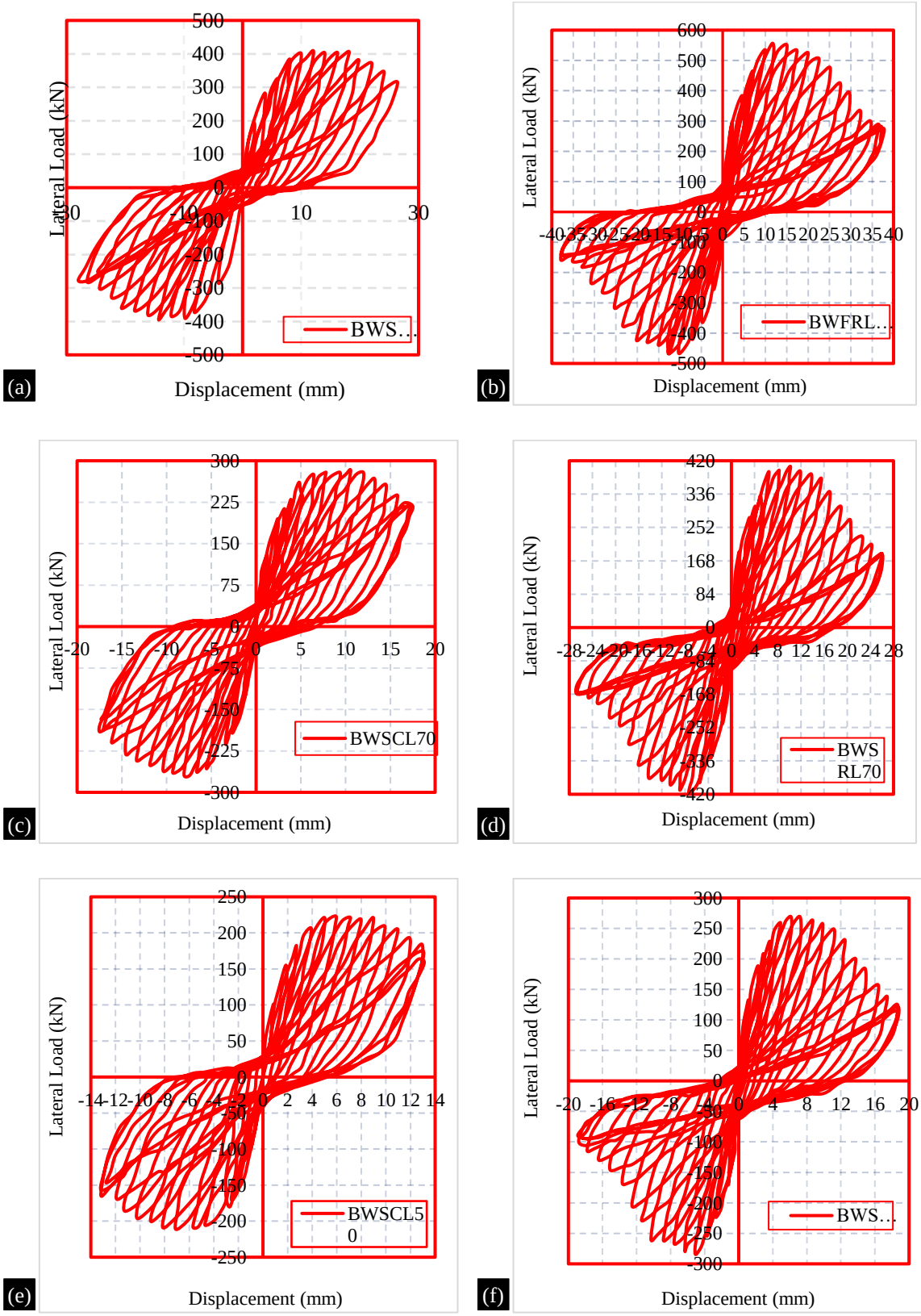

Figure 8. (a) Lateral Load vs. Displacement (BWSCL100) (b) Lateral Load vs Displacement (BWSRL100) (c) Lateral Load vs. Displacement (BWSCL70) (d) Lateral Load vs. Displacement (BWSRL70) (e) Lateral Load vs. Displacement (BWSCL50) (f) Lateral Load vs. Displacement (BWSRL50).

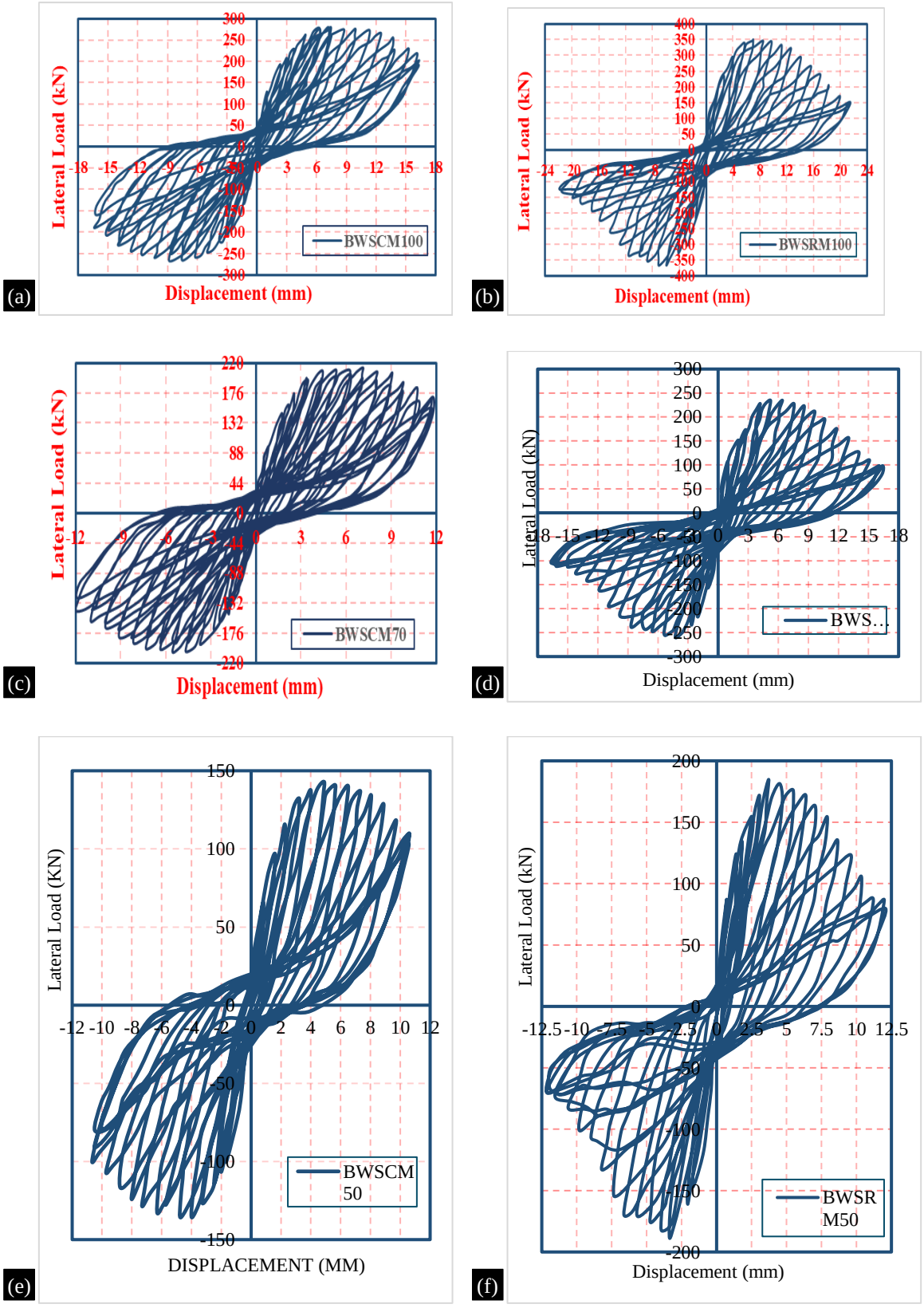

Figure 9. (a) Lateral Load vs. Displacement (BWSCM100) (b) Lateral Load vs. Displacement (BWSRM100) (c) Lateral Load vs. Displacement (BWSCM70) (d) Lateral Load vs. Displacement (BWSRM70) (e) Lateral Load vs. Displacement (BWSCM50) (f) Lateral Load vs. Displacement (BWSRM50).

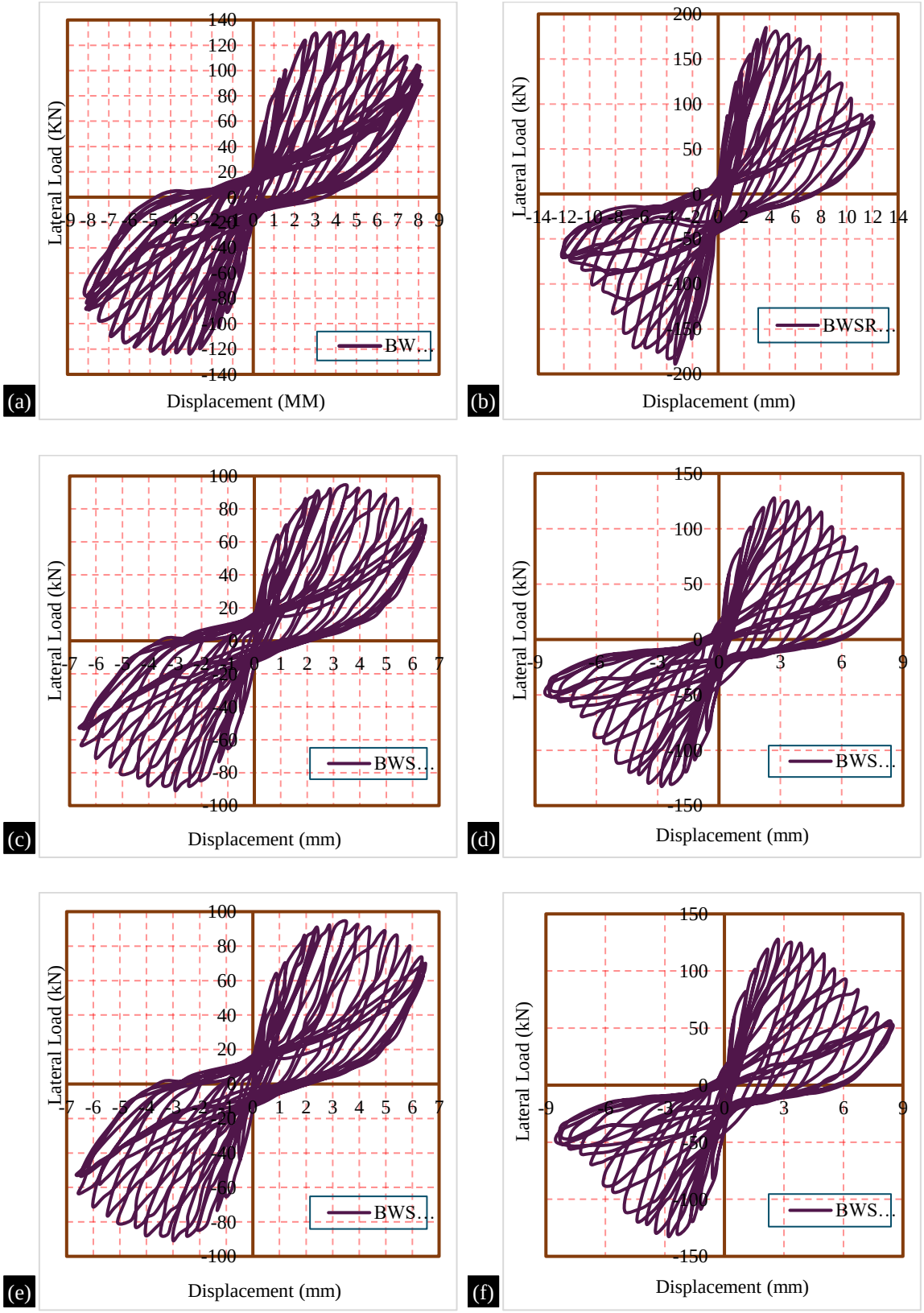

Figure 10. Lateral Load vs. Displacement for all Scale specimens. (a) Lateral Load vs. Displacement (BWSCS100) (b) Lateral Load vs. Displacement (BWSSRS100) (c) Lateral Load vs. Displacement (BWSCS70) (d) Lateral Load vs. Displacement (BWSRS70) (e) Lateral Load vs. Displacement (BWSCS50) (f) Lateral Load vs. Displacement (BWSRS50).

Table 8 showcases the maximum lateral load and maximum displacement for all the specimens under the cyclic load after numerically investigated using ANSYS mechanical APDL. The specimen with the maximum displacement of 37.72 mm is BWFRL100, while the specimen with the minimum displacement of 4.28 mm is BWFCS50.The specimen with the maximum lateral load of 556.15 kN is BWFRL100, while the specimen with the minimum lateral load of 71.03 kN is BWFCS50.In terms of displacement, there is a significant difference between the maximum and minimum values, indicating a wide range of performance among the specimens. In terms of lateral load, the difference between the maximum and minimum values is also significant, suggesting varying levels of resistance among the specimens.

The results from the data provided show a variety of performances across the different specimens when it comes to displacement and lateral load capacity.

Displacement: The displacement values range from a minimum of 4.28 mm (BWFCS50) to a maximum of 37.72 mm (BWFRL100). This wide range suggests that the specimens have different levels of flexibility or elasticity. Specimens with higher displacement values are more flexible or elastic, allowing them to deform more under stress without breaking. GFRP wrapping helped to achieve flexibility too.

Lateral Load: The lateral load capacity also varies significantly among the specimens, ranging from 71.03 kN (BWFCS50) to 556.15 kN (BWFRL100). This indicates that the specimens have different levels of strength or resistance to lateral forces. Specimens with higher lateral load values are likely to be stronger and more resistant to lateral forces.

Correlation: Specimens with higher displacement values tend to have higher lateral load capacities. This could suggest that more flexible or elastic specimens are better able to absorb and distribute lateral forces, resulting in higher resistance and load capacity.

Inter-specimen Comparison: When comparing specimens, BWFRL100 shows the highest performance in both displacement and lateral load, suggesting it might be the most flexible and strongest among the specimens. On the other hand, BWFCS50 has the lowest value, indicating it might be the least flexible and weakest.

Table 8. Maximum Displacement and Maximum lateral load values for all specimens.

S.N.	Specimens	Maximum Displacement (mm) (+)	Maximum Lateral Load (kN) (+)
1	BWFCL100	26.40	408.17
2	BWFCL70	17.51	283.18
3	BWFCL50	13.11	223.44
4	BWFRL100	37.72	556.15
5	BWFRL70	26.10	405.88
6	BWFRL50	26.19	441.43
7	BWFCM100	16.31	280.71
8	BWFCM70	11.90	213.09
9	BWFCM50	10.60	142.97
10	BWFRM100	21.5	348.8
11	BWFRM70	16.42	234.93
12	BWFRM50	12.08	184.85
13	BWFCS100	8.14	130.38
14	BWFCS70	6.51	94.54
15	BWFCS50	4.28	71.03

S.N.	Specimens	Maximum Displacement (mm) (+)	Maximum Lateral Load (kN) (+)
16	BWFRS100	12	185
17	BWFRS70	8.4	127.4
18	BWSRS50	5.6	91

From these results, it can be observed that the size of the specimens (scale) has a significant influence on both the displacement and lateral load. As the scale of the specimen decreases, both the displacement and lateral load tend to decrease on a scale. This suggests that specimens' strength capacity to withstand lateral loads is achieved for varying scales.

CONCLUSIONS

In this study, the performance of exterior beam-column joint with controlled and retrofitted detailing was observed. The following conclusions are drawn from the numerical investigation:

- The failure is observed at the joint under cyclic loading in BCJ specimens.
- Failure at the joint is observed even in the shear reinforcement deficient beam. The shear cracks for BWS specimens are observed.
- As the load increases deflection also increases for all the specimens. Therefore, retrofitted specimens have shown load carrying capacity. With increasing load, the stiffness of all the specimens is gradually decreased.
- . It is observed, shear strength increases with increasing drift ratio for all the specimens. Due to high ductility BWSCL100 showcased significant shear strength as it is designed as per the codal provisions.
- In ANSYS analysis, due to hinge action beams got deflected.
- Size effect can be observed in the specimens from the results.
- GFRP wrapping shows significant strengthening on the Beam weak in shear and it enhances the shear capacity of beam in beam column joints.

The numerical investigation into BCJs performance, investigating controlled and retrofitted detailing, provides significant insights. Despite variations in specimen setups, failure predominantly occurs at the joint during cyclic loading, even when beams lack sufficient shear reinforcement, as indicated by shear cracks in some cases. Additionally, as load increases, deflection rises across all specimens, with retrofitted ones demonstrating improved load-bearing capacity. However, this increased load is accompanied by a gradual stiffness decrease in all specimens. Significantly, shear strength increases with drift ratio, highlighting the importance of ductility in structural resilience. ANSYS analysis underscores beam deflection due to hinge action, while findings reveal a size effect, illustrating the impact of structural dimensions on performance. Particularly noteworthy is the substantial enhancement in shear capacity seen in beam-column joints with GFRP wrapping, especially on weakened beams, emphasizing its effectiveness in strengthening. These results emphasize the complex dynamics governing BCJ behavior under cyclic loads, underscoring the need for tailored retrofitting strategies informed by factors like size effects to enhance structural integrity and resilience.

REFERENCES

1. A. Ghobarah and A. Said, "Shear strengthening of beam-column joints," *Eng. Struct.*, vol. 24, no. 7, pp. 881–888, 2002, doi: 10.1016/S0141-0296(02)00026-3.
2. A. Portillo and L. Moya, "Seismic Risk Regularization for Urban Changes Due to Earthquakes: A Case of Study of the 2023 Turkey Earthquake Sequence," *Remote Sens.*, vol. 15, no. 11, 2023, doi: 10.3390/rs15112754.
3. A. Ghobarah and T. El-Amoury, "Seismic rehabilitation of beam – column joint using GFRP sheets," *Eng. Struct.*, vol. 24, pp. 1397–1407, 2002.
4. L. N. Lowes and A. Altoontash, "Modeling Reinforced-Concrete Beam-Column Joints Subjected to Cyclic Loading," *J. Struct. Eng.*, vol. 129, no. 12, pp. 1686–1697, 2003, doi: 10.1061/(asce)0733-

9445(2003)129:12(1686).
5. J. W. Park, D. H. Kim, S. G. Yoon, and J. Y. Lee, "Shear Deterioration of Reinforced Concrete Beam-Column Joints," *15th World Conf. Earthq. Eng. Lisbon Port.*, 2012.
6. S. R. Uma and S. K. Jain, "Seismic design of beam-column joints in RC moment resisting frames - Review of codes," *Struct. Eng. Mech.*, vol. 23, no. 5, pp. 579–597, 2006, doi: 10.12989/sem.2006.23.5.579.
7. A. Mukherjee and M. Joshi, "FRPC reinforced concrete beam-column joints under cyclic excitation," *Compos. Struct.*, vol. 70, no. 2, pp. 185–199, 2005, doi: 10.1016/j.compstruct.2004.08.022.
8. C. Lima, E. Martinelli, and C. Faella, "Capacity models for shear strength of exterior joints in RC frames: State-of-the-art and synoptic examination," *Bull. Earthq. Eng.*, vol. 10, no. 3, pp. 967–983, 2012, doi: 10.1007/s10518-012-9340-4.
9. S. Sohailuddin and M. G. Shaikh, "Finite Element Modeling of Reinforced Concrete Beam Column Joint Using Ansys," *Int. J. Struct. Civ. Engg. Res.ijscer.com*, vol. 2, no. 3, pp. 2319–6009, 2013, [Online]. Available: http://www.ijscer.com/uploadfile/2015/0429/20150429074659442.pdf
10. B. Venkatesan, R. Ilangovan, P. Jayabalan, N. Mahendran, and N. Sakthieswaran, "Finite Element Analysis (FEA) for the Beam-Column Joint Subjected to Cyclic Loading Was Performed Using ANSYS," *Circuits Syst.*, vol. 07, no. 08, pp. 1581–1597, 2016, doi: 10.4236/cs.2016.78138.
11. I. Factor, N. NAVEEENA, and M. RANJITHAM, "Numerical Study on Retrofitting of Beam Column Joint Strengthened With Cfrp," *Int. Res. J. Eng. Technol.*, vol. 03, no. 01, pp. 914–920, 2016.
12. K. Mary and J. Thompson, *ANSYS Mechanical APDL for Finite Element Analysis*. 2017.
13. M. Kisan, S. Sangathan, J. Nehru, and S. G. Pitroda, "IS 456 (2000): Plain and Reinforced Concrete - Code of Practice [CED 2: Cement and Concrete]," 2000.
14. IS 13920, "Ductile Design and Detailing of Reinforced Concrete Structures Subjected to Seismic Forces Code of Practice (First Revision) ICS," no. July, 2016.
15. IS 456, "sp:16-1980_Design Aids for Reinforced Concrete to IS:456-1978," *Bur. Indian Stand. New Delhi*, p. 232, 1978.
16. ASTM, "ASTM E2126 Standard Test Methods for Cyclic (Reversed) Load Test for Shear Resistance of Vertical Elements of the Lateral Force Resisting Systems for Buildings," no. C, pp. 1–14, 2015, doi: 10.1520/E2126-11.2.
17. Gandhi S, Sheeju Selva Roji S, Motta M, Nalawade RR, Khan MA, Palanisamy S. Analysis of potential incorporation of waste into asphalt pavements. Materials Today: Proceedings,2024.
18. Bahoria BV, Ranjith A, Laxmaiah G, Solomon Raj S, Padhi MR, Palanisamy S. Verification of the mechanical behavior of concrete with partial replacement of the fiber resulting from tire retreading. *Materials Today: Proceedings*. 2024.
19. Palanisamy S, Murugesan TM, Palaniappan M, Santulli C, Ayrilmis N. Fostering sustainability: The environmental advantages of natural fiber composite materials – a mini review. *environmental Research and Technology*, 2024;7(2):256-269.
20. Palanisamy S, Vijayananth K, Murugesan TM, Palaniappan M, Santulli C. The prospects of natural fiber composites: A brief review. *International Journal of Lightweight Materials and Manufacture*. 2024;7(4):496-506.

